To appear in the Astrophysical Journal

EMISSION LINE GALAXIES AT 9200 ≈, INCLUDING A MULTI-COMPONENT GALAXY SYSTEM AT $z = 6.43$

SIMON J. LILLY[1,2], KIM-VY H. TRAN[2], MARK BRODWIN[1,3], DAVID CRAMPTON[1,4], STEPHANIE JUNEAU[4] AND HENRY J. MCCRACKEN[5]

Received 2003 April 17; accepted 2003 July 10;

ABSTRACT

We have carried out a survey for emission line galaxies in the 9200 ≈ atmospheric window using an optimized technique that combines dispersed spectra, multiple parallel long slits and a band-width limiting filter that allows us to cover 8 arcmin^2 to a limit of 2.5 x 10^{-17} erg s^{-1}cm^{-2}. A total of 11 emission line galaxies were detected. Deep *UBVRIZ* photometric data for 10 of these establish unambiguously that they are at $z < 3$. In most cases, the photometric redshift estimate from these data is accurate enough to reliably identify the emission line as either Hα, Hβ and/or [OIII]4959, 5007, or [OII] 3727. These galaxies have the colors expected of star-forming galaxies and show a rough magnitude-redshift relation and a trend of increasing observed equivalent width in the line with redshift. Observed equivalent widths as high as 200 ≈ are seen for these objects. The eleventh emission line object has no detectable continuum shortward of the Z'-band, and is an excellent candidate for a system at $z = 6.43$. Inspection of the spectrogram and the deep images of this region suggest that this galaxy is one of an extended chain of four objects, all visible in Z' but not in I or below. One of these companions has detectable line emission at the same wavelength as the primary. It is concluded that these galaxies likely form an extended linear protogalactic system with a size of 5 arcsec (a proper size of 30 kpc at $z = 6.43$). The extent of this system probably would not have been recognized in a survey involving significant amplification by gravitational lensing. The extended linear geometry is reminiscent of early predictions for protogalactic objects in CDM cosmogonies.

subject headings: *cosmology: observations ñ early universe ñ galaxies: distances and redshifts ñ galaxies: evolution ñ galaxies: formation*

[1] Visiting astronomer at the Canada-France-Hawaii Telescope, operated by the National Research Council of Canada, the Conseil Nationale de recherchÈscientifique and the University of Hawaii.

[2] Department of Physics, Swiss Federal Institute of Technology (ETH Zurich), ETH Hˆnggerberg, CH-8093 Zurich, Switzerland.

[3] Department of Astronomy and Astrophysics, University of Toronto, 60 St. George Street, Toronto, Ontario M5S 3H8, Canada

[4] Herzberg Institute of Astrophysics, National Research Council of Canada, 5071 West Saanich Road, Victoria, British Columbia V9E 2E7, Canada

[5] Osservatorio Astonomico di Bologna, Bologna, Italy

1. INTRODUCTION

Surveys for emission line galaxies are an efficient way to find high redshift galaxies that are in many ways complementary to searches based on the ultraviolet continuum shape as defined by broad band colors, i.e. the Lyman break ìdrop-outî technique (Steidel et al 1996). Many of the highest redshift galaxies have been found in this way (e.g. Ellis et al 2001, Rhoads & Mulhotra 2001, Hu et al 2002, Kodaira et al 2003, see also Cuby et al 2003)

At high redshifts, $z > 5$, ground-based surveys are quite severely limited by the strong OH atmospheric airglow. However, the small atmospheric window between 9000-9300 ≈ that is largely free of OH and other atmospheric lines allows searches for Lyα at $z \sim 6.5$. This is the last such window shortward of 1 μm, although there are others at longer wavelengths in the infrared bands. For the ìconcordanceî cosmology of $H_0 = 70$ kms^{-1}Mpc^{-1}, $\Omega_m = 0.25$ and $\Omega_\Lambda = 0.75$ that is used throughout this paper, the Universe at $z \sim 6.5$ is seen only 0.9 Gyr after the Big Bang, i.e. at 6.5% of its present age. In terms of the $(1+z)$ factor that drives the development of structure in the Universe, the redshift $z = 6.5$ represents as big a step beyond the $z \sim 3$ of the classic ìLyman Break Galaxiesî (LBG) discovered in the mid-1990ís (Steidel et al 1996) as does that from $z \sim 1$. Accordingly, major changes in the galaxy population at these redshifts are expected, even relative to the $z \sim 3$ population, and any information on the nature of galaxies at this epoch is potentially of immense value in understanding, both observationally and theoretically, the formation of galaxies in the Universe.

The significance of this particular redshift is further emphasized by the recent indications from SDSS quasar spectra (e.g. Becker et al 2000) of a strong increase in the HI optical depth at $z \sim 6$. This suggests that we may be approaching the epoch at which the re-ionization of the Universe was completed. The recent detection of a foreground $\tau \sim 0.17$ by the WMAP satellite (Kogut et al 2003) suggests that the period of reionization may have been significantly extended (see also Cen 2002). Reionization and the associated reheating of the intergalactic medium undoubtedly played an important role in the interaction of baryons with growing dark matter haloes, but little is known about the sources responsible for reionization. It is unlikely that quasars were responsible (Fan et al 2001) but the relative role of high and low luminosity galaxies is unknown. Little is also currently known at these redshifts about the role of objects of different luminosities in polluting the intergalactic medium with heavy elements. Observations of the luminosity function and of the astrophysics of individual objects will play a decisive role in addressing these questions.

For all of these reasons, several groups are now actively searching for emission line galaxies at this redshift. The first galaxy at $z > 6$, HCM6A (Hu et al 2002) at $z = 6.56$, was found through a narrow band imaging search behind the lensing cluster A370. Recently, it has been joined by two unlensed objects, also found through narrow-band imaging in the Subaru Deep Field (Kodaira et al 2003) and a system found at $z = 6.17$ (Cuby et al 2003) through narrow-band imaging of the continuum. However, some emission line searches have been unsuccessful. For instance, Ellis et al (2001) did not find galaxies at $z > 6$ in their long-slit search of the small highly amplified regions along lensing-cluster critical lines.

In addition to emission line searches just below $z \sim 6$ (Rhoads & Mulhotra 2001), several groups have also identified possible $z > 5$ galaxies through broad-band search techniques based on HST/ACS *i* and *z* data (Yan et al 2002, Stanway et al 2003) some of which are now being confirmed spectroscopically (Lehnert & Bremer 2002, Bunker et al 2003).

Emission line searches naturally will detect also galaxies at lower redshifts. For emission lines in this window, the most likely low redshift identifications are Hα at $z \sim 0.39$, Hβ and/or [OIII] 4959, 5007 at $z \sim 0.82$ and [OII] 3727 at $z \sim 1.45$. For normal galaxies, there are not expected to be strong emission lines between [OII] 3727 and Lyα although for AGN the CIV 1549 ($z \sim 4.9$) and HeII 1640 ($z \sim 4.6$) are also possibilities (see e.g. McCarthy 1993, Steidel et al 2002, Stern et al 1999). Although the primary motivation for emission line surveys are the very high redshift galaxies, the foreground interlopers are of considerable interest in their own right. Not least for the [OII] 3727 selected sample at $z \sim 1.45$, the Hβ and [OIII] lines are in the *J*-band and Hα is in the *H*-band allowing use of emission line gas metallicity estimators, thereby potentially filling in the gap that currently exists between the $z \sim 1$ samples (Carollo and Lilly 2001, Lilly et al 2003) and the $z \sim 3$ samples (Pettini et al 2001).

In this paper we exploit a technique that combines many of the attractive aspects of narrow-band filter and long-slit dispersed surveys to construct a flux-limited emission line sample at 8971-9246 ≈. These initial data were intended primarily to establish the viability of this technique prior to its application on 8-m class telescopes but has already produced a useful sample of objects, including one interesting multi-component system at $z = 6.43$.

2. OBSERVATIONS

2.1 A new hybrid survey technique

Most of the surveys for high redshift emission line galaxies have been based on narrow-band imaging through filters of width $\Delta\lambda \sim 100$-200 ≈ (e.g. Hu et al 1998, 1999, 2002, Rhoads & Malhotra

2000, 2001, Kodaira et al 2003). Dispersing the light with a spectral resolution that is better matched to the width of the line (i.e. $\delta\lambda \sim 10$ ≈) offers a number of advantages: (a) a potentially large gain in sensitivity by a factor of $(\Delta\lambda/\delta\lambda)^{0.5}$ due to the lower background; (b) the elimination of the effective limit in equivalent width that is introduced by the photometric differencing approach in classic narrow-band filter searches; (c) the ability to increase in the redshift interval that can be surveyed without compromising sensitivity, and (d) the determination of accurate redshifts from the initial spectroscopic survey data.

Long-slit dispersed surveys, either of the directed (e.g. Ellis et al 2001) or serendipitous (e.g. Dey et al 1998) kind have the potential drawback that only a small area on the sky can be observed at a given time. However, the use of a band-width limiting filter allows multiple parallel long-slits to be used (see Crampton and Lilly 1999, Stockton 1999). With modern wide-field spectrographs, an area of several arcmin^2 can be surveyed simultaneously at the cost, of course, of spectral coverage. For many purposes, this is an acceptable trade, given the difficulty of using data in the surrounding OH forest and, at least for galaxies at $z \sim 6.5$, the fact that no emission is expected at wavelengths below the emission line anyway.

Choice of the spectral resolution used in this technique represents a trade-off between sensitivity and the ability to recognize lines from asymmetric profiles (e.g. Lyα) or doublets (e.g [OII] 3726, 3729) on the one hand and a reduction in surveyed area on account of the longer spectra on the other.

In this paper we analyze data from an exploratory survey using this technique on the 3.6m Canada-France-Hawaii Telescope (CFHT) in the CFRS-2215+00 field. A crucial aspect of this program is the use of deep multi-color *UBVRIZ'* photometry to generate photometric redshift estimates and thus to identify the emission lines.

2.2 Spectroscopic survey observations and data reduction

The spectroscopic survey observations were carried out during the nights of 1998 20-22 August using the MOS side of the MOS/SIS spectrograph on the CFHT. The R150 grating and STIS2 CCD detector gave a plate scale of 0.44 arcsec pixel^{-1} and 10.5 ≈ pixel^{-1} in the dispersion direction. The resolving power is about 460 for 0.9 arcsec seeing. Although probably non-optimal in terms of resolution, this was the highest resolution red-sensitive grism available on MOS/SIS at the time. A custom filter 300≈ wide centered on 9130≈ was used to limit the spectra to about 30 pixels in the dispersion direction. The focal plane multi-slit mask had 29 parallel slits each 506 arcsec long and 2 arcsec (5 pixels) wide, except for those at the very top and bottom which were truncated by the mask holder. These parallel slits were cut 17.2 arcsec apart (i.e. 39 pixels at the detector). The slit spacing was chosen to be slightly larger than the length of each spectrum so that the zeroeth order spectra from the slits at the top of the mask fell into the gaps between the first-order spectra from slits below. In cutting the slits, two small ìbridgesî were left across each slit to increase the structural integrity of the mask. An image of this mask has been shown in Crampton & Lilly (1999).

The total area covered by open slits is 8.0 arcmin^2. With a 260 ≈ spectral range (see below) the volume corresponds to 240 comoving Mpc^3 at z = 0.39, 1990 Mpc^3 at z = 1.45 and 5100 Mpc^3 at z = 6.5. At $z \sim 0.84$, the redshift interval is broader because of the multiple lines, $\Delta z \sim 0.21$, giving a comoving volume at this redshift of 3400 Mpc^3.

A total of 13 integrations each 3600 sec long were obtained with this slit-mask. The slits were aligned East-West, and small offsets were made along the slit direction to allow the identification and removal of instrumental artifacts, including variations in the slit profile and the usual CCD flat-field pattern as well as the shadowing from the small ìbridgesî in each slit. A spectrum from an Argon arc lamp was taken to provide a wavelength calibration and in particular to facilitate removal of the pin-cushion distortion in the MOS.

Data processing was carried out under the IRAF environment. Following standard bias and dark subtraction, the y-component of the distortion was removed from each data frame. Each science image was then flattened with a ìsky-flatî generated from a median average of normalized versions of the twelve other science images. This ìsky-flatî thus includes the effects of the imperfect cutting of the slits and of the CCD flat-field pattern $f(x,y,\lambda)$.

Prior to the registration and co-addition of the frames, a sky background was computed and subtracted for each row of the data (i.e. constant wavelength) using a running window of 40 arcsec. The 13 science frames were then combined using a bad pixel mask for both the shadows from the bridges and CCD bad columns. At this point also, the wavelength range was trimmed to a 260 ≈ range between 8986-9246 ≈.

Flux calibration of the data was achieved through several observations of the Kitt Peak standard star Feige 24. Because of the band-width limiting filter, the calibration curve changes quite sharply across the accessible wavelength range. This is a concern for any objects that were not centered in the slit, since they will be flux calibrated using a calibration curve that is slightly offset in wavelength, possibly producing the appearance of spurious low equivalent width emission lines at the edge of the band-pass. This effect was reduced through our spectral trimming. Inspection of the individual

objects makes us confident that none of the claimed emission lines are artifacts of the flux calibration.

The observing and reduction process, coupled with the absence of bright OH skylines in the spectral window, produced a final image that was exceptionally clean and free of any obvious defects, with only a small variation in noise associated with the mild variations of the sky brightness with wavelength across the final selected wavelength interval.

At this point, the continua from approximately 100 objects were visible on the co-added spectrogram. The final processing step for the spectroscopic data was to remove these continua from the image, leaving a 2-dimensional ìline-imageî in which emission lines appear as small point-like sources. This continuum subtraction was achieved by fitting a first-order polynomial to the brightness in each column (i.e. parallel to the dispersion direction) and subtracting the resulting ìcontinuum-imageî from the data. The continuum image was then used to determine the continuum brightness of objects and the equivalent width of the emission lines. Not surprisingly, this continuum subtraction process was not perfect, especially for some of the brighter objects, because of features in the continuum within the spectral window. However, the objects in which the continuum did not perfectly subtract were easily recognizable because the residuals were elongated along the spectrum and frequently were both positive and negative, whereas genuine emission lines were, at this spectral resolution, quite symmetrical in x and y.

A catalogue of emission line objects was generated using Sextractor, and from this a final catalogue of objects was produced which were confirmed by several independent visual inspections of the data to eliminate spurious continuum-subtraction artifacts. The 1σ noise over most of the final image are 0.5×10^{-17} erg s^{-1} cm^{-2} in a 2 arcsec diameter aperture. A 5σ detection was regarded as secure and this limit is taken as the reasonable completeness limit. Unexpectedly, three of the objects with the lowest equivalent width emission features ($W << 10$ ≈) were identified with M stars. These were recognized through their compact profile and *UBVRIZ′* colors. This feature is probably the CN feature seen at 9200 ≈ in the comparable resolution spectral atlas of Pickles (1985). The final sample of emission line galaxies consists of 11 galaxies (i.e. 1.4 arcmin^{-2} or 5.3×10^{-3} arcmin^{-2}≈$^{-1}$) above $f > 2.5 \times 10^{-17}$ erg s^{-1} cm^{-2}. All except the brightest galaxy have $W_0 >> 10$ ≈. These are listed in Table 1, catalogued for convenience with an LTBC number.

2.3 Deep imaging data

The CFRS-2215+00 field has been observed as part of the Canada-France Deep Fields (CFDF) survey program and deep images are available in six bands *UBVRIZ′* (Brodwin et al 2003). These reach a limiting magnitude (2σ in 2 arcsec apertures) of U_{AB} = 27.00, B_{AB} = 26.25, V_{AB} = 26.35, R_{AB} = 26.5, I_{AB} = 26.45, Z'_{AB} = 25.55. The reduction of these images followed standard procedures (McCracken et al 2001, Brodwin et al, in preparation).

Well over 100 objects were detected in the continuum in the spectroscopic data and these could readily be identified on the deep images. This allowed a precise transformation to be constructed between the spectroscopic and imaging data. Consequently, the location of the 29 slits on the CFDF images could be reconstructed post facto. The result is that, folding in the 2 arcsec width of the slit, there is for a given pixel in the spectrographic data a maximum positional uncertainty in the broad-band images of ±0.5 arcsec in right ascension, and ±1.0 arcsec in declination. This was sufficient to unambiguously identify the objects responsible for the emission lines on the deep imaging data. Coordinates and photometry for these are given in Table 1. For a given pixel in the spectrogram, there is a ± 25 ≈ ambiguity in wavelength for a given pixel depending on the location of the object in the slit.

An inevitable feature of this long-slit survey technique is that many objects are not wholly within the slit. In future applications, stepping of the mask across the sky will remove this problem. The continuum AB magnitude (in a 2×2 arcsec^2 square aperture) derived from the spectra is compared with the Z'_{AB} photometry from the imaging data (2 arcsec diameter circular aperture) in Table 1. At bright levels, the objects scatter faintwards by up to 1.5 magnitudes from the nominal brightness. At the faintest levels there is little systematic offset, presumably because non-optimally placed objects fall below the detection threshold.

3. PHOTOMETRIC REDSHIFTS AND IDENTIFICATION OF EMISSION LINES

As noted above, there are several possibilities for a bright emission line at λ ~ 9200 ≈. Apart from Lyα at z ~ 6.5, the most likely possibilities are Hα at z ~ 0.4, Hβ or [OIII] 4959,5007 at z ~ 0.85 or [OII] 3727 at z = 1.45. In the case of one galaxy (LTBC-6), three emission lines are visible in our spectral window and so these can be securely identified with Hβ and [OIII] 4959,5007. However, the filter passband is narrow enough that in either Hβ or [OIII] 5007 might appear on their own so the appearance of just a single line does not exclude this identification.

The *UBVRIZ′* photometry can be used to discriminate between these possibilities ñ either through simple detection of continuum in the *I*-band or shorter, to rule out z ~ 6.5, or through photometric

TABLE 1

LTBC	[2000] RA	[2000] dec	λ(≈) (a)	f_{line} (b)	$Z'_{AB,cont}$ (c)	W_{obs} (d)	z (e)	2 arcsec aperture photometry U_{AB}	B_{AB}	V	R_{AB}	I_{AB}	Z_{AB}
18b	22 17 40.15	+00 20 19.1	9119	7.4	23.23	101	1.45	24.08 ±0.0	24.25 ±0.08	24.10 ±0.08	23.81 ±0.05	23.65 ±0.05	23.50 ±0.09
18a	22 17 40.29	+00 20 20.6	9140	4.3	23.63	85	1.45	23.92 ±0.03	23.89 ±0.06	23.74±0.06	23.75 ±0.05	23.56 ±0.04	23.18 ±0.06
15	22 17 47.63	+00 20 35.4	9130	2.2	25.29	200	1.45?	$25.86^{-0.18}_{+0.22}$	$25.98^{-0.36}_{+0.54}$	$25.52^{-0.26}_{+0.35}$	$26.14^{-0.36}_{+0.53}$	$25.18^{-0.17}_{+0.20}$	$25.59^{-0.48}_{+0.87}$
14	22 17 52.40	+00 14 52.8	9151	5.8	22.43	38	0.84	24.94 ±0.08	24.87 ±0.14	24.20 ±0.18	23.57 ±0.04	23.00 ±0.03	22.75 ±0.05
13	22 17 53.50	+00 19 25.5	9098	3.9	22.54	28	0.40	23.71 ±0.03	23.37 ±0.04	22.77 ±0.03	22.48 ±0.02	22.45 ±0.02	22.24 ±0.03
12	22 17 59.24	+00 19 58.0	9204	3.0	23.14	38	0.84	24.87 ±0.07	24.36 ±0.08	24.52 ±0.11	24.14 ±0.07	23.37 ±0.04	23.09 ±0.06
11	22 17 59.65	+00 20 15.5	9204	3.8	23.19	50	0.84?	25.18 ±0.10	24.73 ±0.13	24.38 ±0.10	24.25 ±0.07	23.71 ±0.05	23.38 ±0.08
8	22 18 04.96	+00 20 49.1	9088	8.2	20.26	7	0.40	23.77 ±0.03	23.05 ±0.03	21.80 ±0.02	21.05 ±0.01	20.47 ±0.01	20.19 ±0.01
6	22 18 06.44	+00 21 05.5	9225	7.7	21.89	30	0.84	23.60 ±0.03	23.39 ±0.04	23.03 ±0.03	22.85 ±0.02	22.44 ±0.02	22.31 ±0.03
3	22 18 06.95	+00 15 23.4	9003	8.1	22.56	60	0.40	25.14 ±0.10	24.73 ±0.13	24.35 ±0.10	24.17 ±0.07	23.83 ±0.05	23.52 ±0.09
4	22 18 07.50	+00 22 13.2	9035	3.0	24.90	200	6.43	> 27.1 (2σ)	> 26.1 (2σ)	> 26.9 (2σ)	> 27.3 (2σ)	> 26.7 (2σ)	$25.70^{-0.52}_{+1.03}$

Notes to Table 1:

(a) Apparent wavelength of line with 25≈ uncertainty.

(b) Apparent flux of line in units of 10^{-17} erg s^{-1} cm^{-2}.

(c) Apparent level of continuum from spectrum. The offset from the photometric Z_{AB} is a measure of the slit losses from mis-centering.

(d) Observed equivalent width of line in ≈.

(e) Redshift is based on line identification from photometric redshift estimate. LTBC-11 and ñ15 have alternate redshifts that are not very much less likely. Justification for redshift of LTBC-4 is given in Section 4.

TABLE 2

LTBC-4	[2000] RA	[2000] dec	aperture	f_{line} (Wm^{-2})	Z_{AB}	$(I\text{-}Z)_{AB}$ median	$(I\text{-}Z)_{AB}$ 84%
A	22 18 07.5	+00 22 13.2	2"	3×10^{-20}	25.7	2.1	> 0.9
B	22 18 07.7	+00:22:14.2	1"	0.5×10^{-20}	26.2	1.5	> 0.6
C	22 18 07.8	+00 22 13.5	1"	Ö	26.2	1.3	> 0.5
D	22 18 07.9	+00 22 13.6	1"	Ö	26.1	2.0	> 1.0

redshifts to potentially differentiate between the above possibilities. Of the 11 objects, all but one are detected in the *U*-band and are thus almost certain to lie at redshifts $z < 3$ ruling out Lyα (as well as HeII 1640 and CIV 1549). For these ten galaxies we have applied a photometric redshift estimator, as described in the next section.

For the remaining object, LTBC-4, no significant detection was made in any of the *UBVRI* filters. The properties of this interesting object are explored in Section 4 in which we argue that it is at $z = 6.43$.

3.1 Photometric redshift estimates

The *UBVRIZ'* photometry for each of the 10 emission line galaxies with detectable continuum in *UBVRI* (i.e. those demonstrably at $z < 3$) has been run through a photometric redshift code (Brodwin et al, in preparation). This has been extensively tested on 332 CFRS galaxies with secure redshifts $0 < z < 1.3$ and $I_{AB} < 22.5$, where it typically produces redshift errors of $\sigma_z < 0.07$ for 93% of the objects. Simulations involving adding scaled versions of the same image to itself suggest that in this field, σ_z is still less than 0.12 for more than 80% of objects at $I_{AB} < 25$. Thus, in the redshift and brightness regime sampled by most of the emission line sample, the photometric redshift scheme should be able to discriminate between the three main emission line possibilities.

The output of the code is a likelihood function for each galaxy as a function of redshift. In this application, we can be quite confident that the redshift should be one in which a bright emission line falls into the observed spectral passband, which limits the redshifts to one of the three choices described above. Accordingly, we need only examine the relative likelihoods of these three possible redshifts. These are illustrated in Fig 1 where the objects from Table 1 have been ordered by their *I*-band magnitude. For 6/10 galaxies there is no ambiguity at all in the correct line identification. For two others, the intermediate redshift ($z \sim 0.84$) is more than twice as likely as any other. In fact for one of these, LTBC-6, we know that this is the correct redshift because all three of Hβ and [OIII] 4959 and 5007 are seen in the spectrum. For the remaining two objects, LTBC-11 and ñ15, which are the faintest, there is a less clear cut indication, with an alternative redshift at comparable likelihood.

Adopting the redshifts indicated by Fig 1 (with alternates for the two faintest galaxies), the magnitude vs. redshift and observed equivalent width vs. redshift diagrams have been constructed in Figs 2 and 3, also including for comparison the $z = 6.43$ system described below. These behave as expected: the continuum brightness decreases and the equivalent width increases with redshift.

It should be noted that LTBC-15 has a relatively high equivalent width (200≈) yet indubitably lies at $z < 3$. Compared with emission line searches at shorter wavelengths, the The higher redshifts that potential "low" redshift lines have in a 9200 ≈ survey compared with one st shorter wavelengths will produce higher equivalent widths. For example [OII] 3727 is at $z \sim 1.4$ as opposed to $z \sim 1$ for searches at 7500 ≈, resulting in a 20% higher equivalent widths. In addition, as the wavelength of the survey increases, a much larger volume is available for lines such as Hα which can also have high equivalent widths (e.g. Stern et al 2000).

With larger samples, one could use these lower redshift objects for studies of the luminosity function

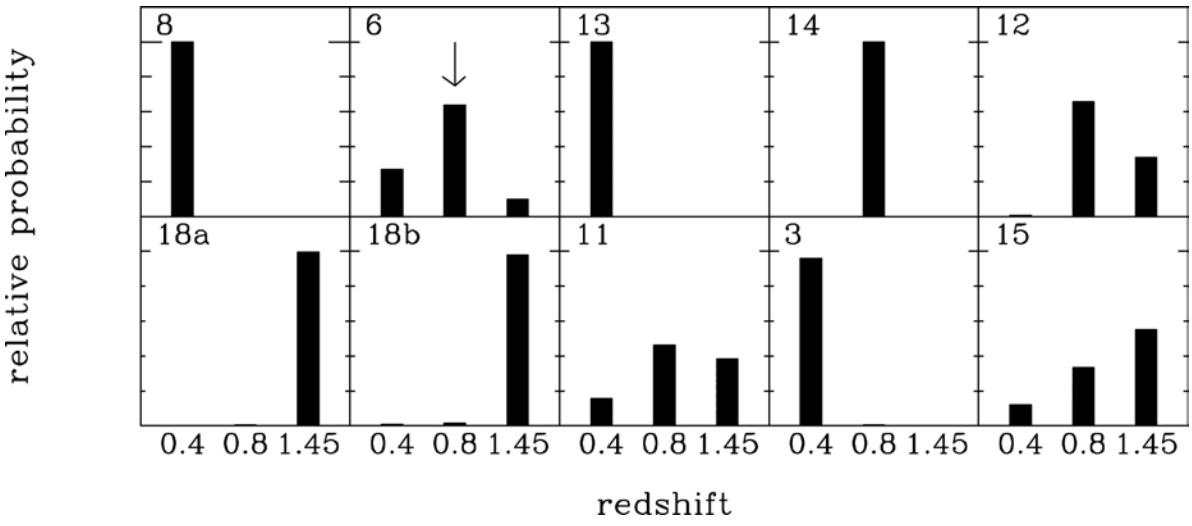

Fig 1 Relative likelihoods of the three possible z < 3 redshifts for the ten emission line galaxies in the present program that were detected in UBVRI. The galaxies are ordered (left to right, top to bottom) in I_{AB} brightness. For six objects there is no ambiguity in the redshift and line identification. The arrow for LTBC-6 indicates that this galaxy is definitely at z = 0.84 based on the presence of Hβ and [OIII] 4959, 5007 in the spectrum. The redshifts of the two of the faintest objects, LTBC-11 and -15, are uncertain between z = 0.84 and z = 1.45.

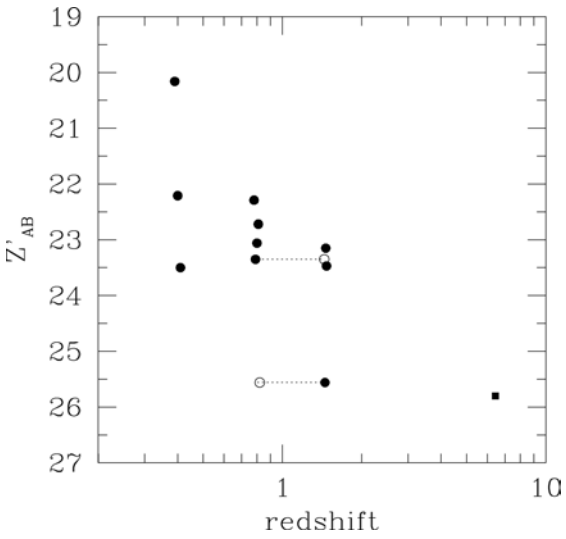

Fig 2. The Z_{AB}-z plot for all eleven galaxies. The galaxies are plotted at the redshift indicated by the line identification from the photometric redshift estimate. For LTBC-11 and LTBC-15, the alternate redshift is shown as an open symbol. The solid square indicates LTBC-4A at z = 6.43.

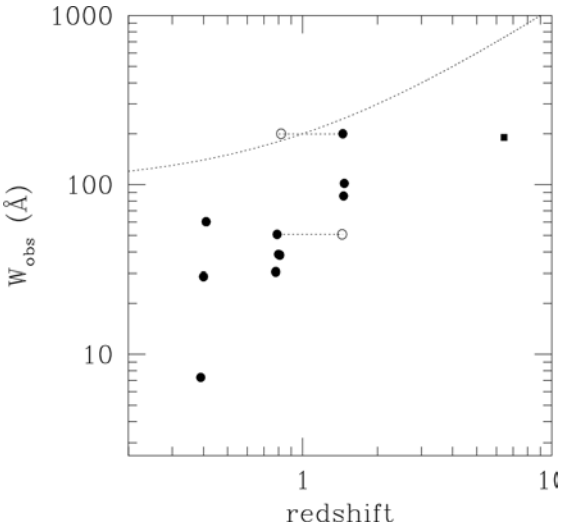

Fig 3. The observed equivalent width W-z plot for all eleven galaxies. This will change with redshift because of the (1+z) cosmological effect and because different lines are observed. The dotted line shows the observed W for a line with rest W_0 = 100 ≈.

and luminosity density in the relevant emission lines at these redshifts. We will defer such analysis until a larger sample is available from our ongoing survey programs.

4. A SYSTEM OF GALAXIES AT A PROBABLE REDSHIFT OF z = 6.43

The remaining object, LTBC-4, has a convincing 7σ detection (Fig 4) of line emission at 9035 ≈. Photometry of the line, without continuum subtraction, gives a measured flux of 3.4 ± 0.45 × 10^{-20} Wm^{-2} in a 2 arcsec aperture. In the spectrum, there is a marginal detection of the continuum, at a level of 1.6 ± 0.8 × 10^{-22} $Wm^{-2}≈^{-1}$ (AB ~ 24.9), in three independent 50 ≈ continuum intervals longward of the line, but not in the 50 ≈ shortward of the line (Fig 5 inset). This continuum may contribute 0.4 ± 0.4 × 10^{-20} Wm^{-2} to the measured line and so we take the most likely line flux to be about 3 × 10^{-20} Wm^{-2}.

The emission line region is just detected in our *Z′*-band image as a small lumpy object about 1.5 arcsec across (the image has 0.5 arcsec seeing). A 2 arcsec aperture measurement gives a detection at an integrated Z'_{AB} = 25.7 (2 arcsec) at 1.6σ.

Nothing is visible at this location in any of the *U, B*, *V*, *R* or *I* images, or on a stack of *B+V+R+I* images which has an effective limiting depth of 27.3 (2σ/2 arcsec) for a flat spectrum object. The absence on the R- and I-band images is quite striking: we derive (Fig 5) a 95% confidence upper limits of I_{AB} > 26.6 and R_{AB} > 26.9. Several arguments ultimately based on the absence of the continuum shortward of the line point towards an identification of this single emission line as Lyα at *z* = 6.43 ± 0.02. In this context, the reader is referred to an extensive discussion of the issues surrounding single line identifications that has been presented by Stern et al 2000).

In developing these arguments from our noisy measurements and upper limits, we have carefully considered the statistics of the measurements. For each observation, we consider all possible (i.e. positive) values of the true brightness of the object, from zero to infinity. For each possible true brightness, we can compute the probability that fluctuations in the sky background would have resulted in the actually observed brightness, i.e. the probability that the background fluctuation would have been equal to the difference between the true brightness in question and the actually observed brightness from that small part of the sky. For this we use the gaussian statistics of the sky background fluctuations, normalized so that the probability integral over all possible true brightnesses of the object is unity. We then examine the probability distribution to derive confidence limits. To derive limits to the colours, we consider all possible pairs of true brightnesses in the two bands using conditional statistics and thus derive the probability distribution of the color. This enables us to identify the "median color" corresponding to the point midway through the probability distribution and an 84% confidence interval as a limit to the color.

The arguments in favor of a Lyα *z* = 6.43 identification for LTBC-4A are as follows:

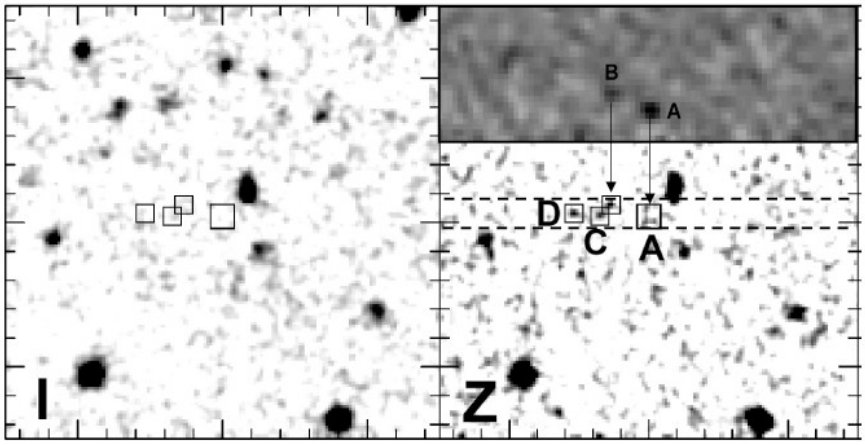

Fig 4 (Right inset) 2-dimensional spectrogram of LTBC-4. The image is orientated with distance along the slit horizontal (total extent 30 arcsec) and wavelength vertical (total extent 260≈, wavelength increasing upwards). The spectrogram shows the highly significant detection of emission line "A" and the much fainter emission "B" 3.5 arcsec to the left. (Right main panel) A 0.5" seeing Z-band image to the same spatial scale and orientation as the spectrogram. This image reveals that "A" comes from a very faint apparently lumpy object that is visible in Z but not in I (left hand panel). The fainter line emission "B" to the ENE is exactly coincident with a faint red object that is also visible in Z but not in I. Finally, two other Z'-band objects further to the East are similarly absent in I. The system spans a total of 5 arcsec (30 kpc at z = 6.43). The axis tick marks are spaced at 2 arcsec and the two horizontal dashed lines in the right hand panel show the location of the spectrograph slit on the sky.

(a) Assuming the spectroscopic continuum above the line is real, it suggests a break across the line of more than 1.9 magnitudes (at 84% confidence). This is as expected for Lyα but would be uncomfortably large for a Balmer break across [OII] 3727 or for the 4000 ≈ break at slightly longer wavelengths.

(b) If we ignore the spectroscopic measurement and look only at the *I* and Z' imaging data, we derive a median $(I\text{-}Z')_{AB} = 2.1$ with $(I\text{-}Z')_{AB} > 0.9$ at 84% confidence. Even this reduced amplitude of the break makes this object quite different from the other 10 emission line galaxies in the sample. This is illustrated in Fig 6 which shows the $(I\text{-}Z')_{AB}$ colors of all eleven objects as a function of their photometrically estimated redshifts. As expected, the lower redshift emission line objects lie in the locus of star-forming galaxies with colors bluer than a local Sbc galaxy. LTBC-4A, however, has colors that are consistent with those expected for a galaxy at $z = 6.43$ and inconsistent with those expected for galaxies at any lower redshift, except for a (rather implausible) unevolved elliptical-like galaxy at $1.8 < z < 2.3$. The line could then conceivably be MgII 2799 at $z \sim 2.23$ although it would need to be considerably stronger ($W_0 \sim 60$ ≈) than usually seen in radio galaxies ($W_0 \sim 20$ ≈, McCarthy 1993).

(c) The observed equivalent width derived from the nominal continuum in the spectrogram measured at wavelengths longward of the line is 190 ≈, similar to the equivalent width in the Hu et al (2002) and Kodaira et al (2003) $z \sim 6.5$ objects. If instead we ignore this measurement and adopt the fainter imaging *Z'*-band level, the equivalent width increases to about 400 ≈, or to 630 ≈ if we average the *Z'* and the *I*-band upper limit. Large equivalent widths can arise from active galactic nuclei, and especially in the extended line emission regions often associated with such objects at high redshift (see e.g. Stern et al 2000 for a cautionary example).

Subsequent inspection of the spectroscopic image (Fig 4) revealed a second region of fainter line emission located about 3 arcsec East along the slit, with $f \sim 0.5 \pm 0.23 \times 10^{-20}$ Wm^{-2} (in a 1 arcsec aperture). If the line has the same wavelength, then it would be exactly coincident with a red galaxy ìBî that is visible on our *Z'* images. Although slightly to the North of East, this object would nevertheless still have been in the 2 arcsec slit. Finally two more red companions ìCî and ìDî lie further to the East. All three objects are clearly present in the *Z'*-band image but are absent in the *I*-band and in all of the other shorter bands (see Fig 4 and Table 2). ìCî and ìDî are not detected in the line emission (or in continuum on the spectrogram). Given the closeness of "B" to "A", an alternative explanation for this system which we cannot at this stage completely rule out is that "B" is an active object at $z \sim 1.4$ and that "A" is an extended emission line region associated with it. However, there are no FIRST radio sources above 1 mJy within 5 arcmin of LTBC-4. Future higher resolution observations of the line should settle this question.

We have computed $(I\text{-}Z')_{AB}$ colors for these objects as above and find median colors of 1.5, 1.3 and 2.0, respectively, and limits (84% confidence) of greater than 0.6, 0.5 and 1.0 respectively. These are

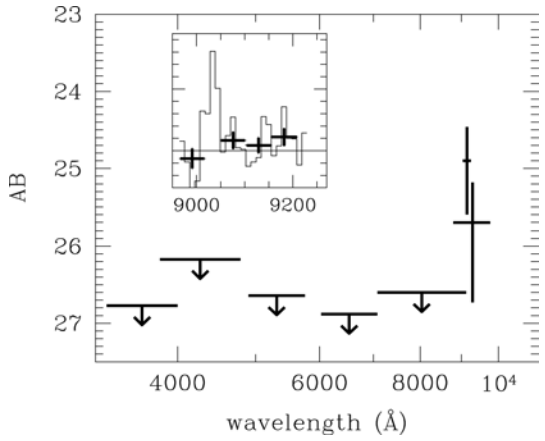

Fig 5 (Inset): Spectrum of LTBC-4A extracted from the spectroscopic data. The continuum is weakly but consistently detected above the line, but not below it. (Main panel): The spectral energy distribution of LTBC-4A derived from the photometric data. The limits are 95% confidence levels for the lack of detection in UBVR and I. The wide bar with error bars (1σ) at λ > 9000 ≈ is the Z-band imaging measurement. The point at 9200 ≈ is based on the continuum detected in the spectrogram. The summed BVRI image has a 95% limit of AB > 27.1.

also plotted on Fig 6. Again, they have the colors expected for galaxies at $z \sim 6.5$ but are much redder than galaxies at almost all lower redshifts.

We believe that by far the most likely interpretation for these four sources ì ABCDî is that they are a string of related proto-galactic objects at $z = 6.43 \pm 0.02$. The dimension of about 5 arcsec end-to-end corresponds to a proper size of 30 kpc at this redshift. The overall linear geometry and physical extent of the system is reminiscent of early simulations of forming galaxies in CDM cosmologies (see e.g. Baron and White 1987, Weinberg et al 2002 and references therein) once the cosmology is corrected to the modern standard model.

An interesting aspect of the extended linear structure of this system is that it would presumably not have been found using techniques that rely on a large degree of gravitational amplification (c.f. Hu et al 2002, Ellis et al 2001) because only part of the system would have been strongly amplified.

Following Hu et al (2002), the Lyα luminosity of "A" would correspond to a star-formation rate (SFR) of about 15 $M_{\odot}yr^{-1}$ based on Kennicutt's (1983) local relation. The continuum levels, though poorly determined should provide a more robust estimate of the unobscured star-formation. The continuum levels of $Z'_{AB} \sim 26$ in these four objects also suggest a SFR ~ 15 $M_{\odot}yr^{-1}$.

Figure 7 shows the observed surface density of this object and those of the few others found hitherto at similar redshifts. The implied surface number density of this single system is broadly consistent with that of the lensed HCM6A unless the luminosity function is very steep. It is somewhat higher than the number densities of the Kodaira et al (2003) objects (unlensed and of similar luminosity to LTBC-4) and of the lower redshift $z \sim 5.7$ LALA sample (Rhoads & Malhotra 2001, 2002) when that is translated to z ~ 6.5 assuming no evolution. LTBC-4 should also have been detected in the unamplified part of the Hu et al (2003) survey, but no such objects were. Thus, assuming our own object is indeed at z = 6.43, we may conclude that we may have been "lucky" to have found it in 8 $armin^2$, but given the small number statistics of all of the studies, we were not so lucky as to cast at this stage serious doubt on the correctness of the identification.

In arguing for the high redshift identification for this object, the absence of detectable continuum shortward of the line has been critical. As noted above, LTBC-15 has a similar line flux, high equivalent width (W ~ 200 ≈ observed) and Z'_{AB} brightness. Unlike LTBC-4A it is however detected all the way down to *U* with AB < 26 with a blue overall color $(U-I)_{AB} \sim 0.7$. This object emphasizes that at this wavelength, which is a bit longer than most previous surveys (thereby producing higher redshifts for the "low redshift" interlopers), high equivalent widths W ~ 200 ≈ are not the exclusive preserve of Lyα galaxies.

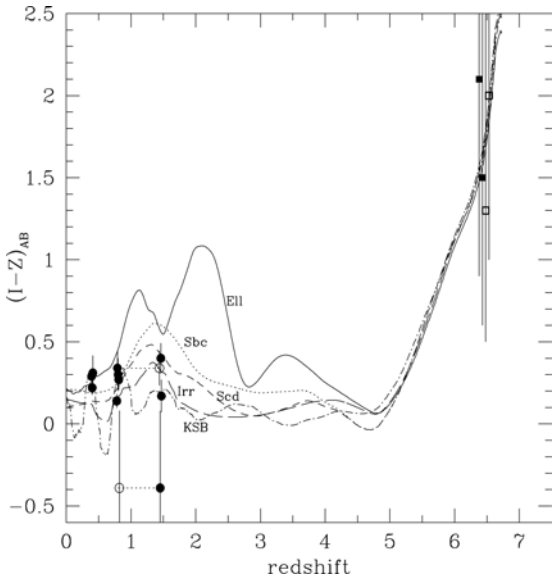

Fig 6 The $(I-Z)_{AB}$ color for galaxies detected in this program compared with the expected colors of standard template galaxies. The low redshift systems have the colors of star-forming galaxies. LTBC-4A has a much redder $(I-Z)_{AB}$ color (leftmost point at high redshift). While this color is matched by an elliptical galaxy at z ~ 2, this would not be consistent with a plausible line identification at 9200 ≈. The three companions to this object, "BCD", one of which also shows line emission, have similarly red colors (remaining high z points, left to right).

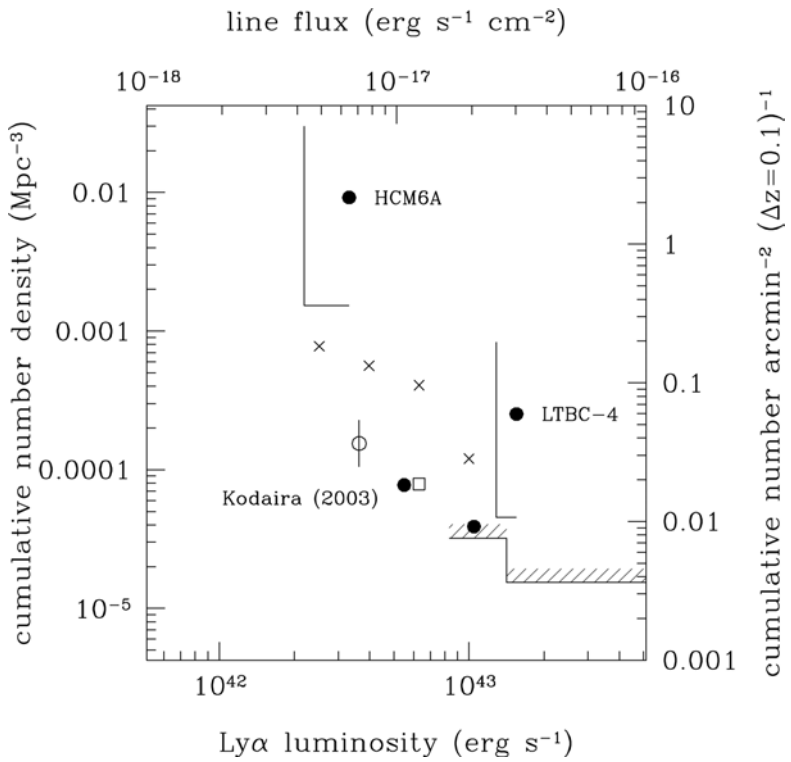

Fig 7. Line brightness and object number densities in observed units for the four galaxies found in the 9200 ≈ window (Hu et al 2002, Kodaira et al 2002 and this work), shown as solid symbols. The top and right hand axes show observed quantities and the bottom and left hand axes show derived physical quantities, assuming z = 6.5 and the concordance cosmology as in the text. For HCM6A and LTBC-4, for which only one object was found, the galaxies are plotted at their actual brightnesses (corrected for lensing in the case of HCM6A), with an associated errorbar drawn at the survey limit. The two Kodaira et al objects are likewise plotted with an additional open circle representing the two additional good candidates found down to the search limit of that survey. The open square represents the 3 confirmed galaxies at z = 5.7 in the LALA survey translated to z ~ 6.5 assuming no evolution. The crosses represent the z ~ 3.5 luminosity function of Hu et al (1999) converted to the assumed cosmology and translated to z ~ 6.5 assuming no evolution. The hatched limit represents the upper limit from the non-detection of objects in the unlensed part of the Hu et al (2002) survey. Given the small numbers involved in all of the surveys, the data are probably consistent with a single luminosity function. Assuming that LTBC-4 lies at z = 6.43, then we were probably "lucky" to find such a bright object in our preliminary proof-of-concept survey.

5. CONCLUSIONS

We have shown that the hybrid "multi-slit plus filter" approach is an effective survey strategy for emission line galaxies in narrow atmospheric windows. We used this technique to survey 8 arcmin^2 to a limiting 5σ depth of 2.5×10^{-17} ergs^{-1}cm^{-2} and found eleven galaxies in a wavelength interval of 260 ≈.

Detection in the *U*-band for ten of the eleven galaxies constrains their redshifts to be at $z < 3$. Photometric-redshifts derived from deep multi-band *UBVRIZ′* photometric data have been used to identify the emission lines as Hα, Hβ or [OIII]4959, 5007, or as [OII] 3727. The low redshift galaxies have the colors of blue star-forming galaxies. The higher redshift objects have fainter continua and higher equivalent widths, as would be expected.

The one remaining emission line galaxy likely has $z = 6.43$. The arguments for the $z = 6.43$ identification are based on the red $(I\text{-}Z')_{AB} > 0.9$ (84% confidence) color, an inferred continuum drop across the line from the spectrogram, and the high equivalent width of the line.

This last galaxy has three close neighbors in a roughly linear pattern spanning 5 arcsec. One of these also shows the emission line at the same wavelength and, like the primary, these three are all detected in *Z′* but not in *I*, or in any other shorter wavelength band, implying $(I\text{-}Z')_{AB} \geq 1$. While other possibilities cannot at this stage be categorically ruled out, the most natural interpretation is that this system is an extended protogalactic complex at $z = 6.43$. In this case the physical extent would be 30 kpc at $z = 6.4$. The implied minimum star-formation rates in each component are of order 15 $M_\odot yr^{-1}$.

We thank the staff at CFHT for their expert assistance with these observations and Marcin Sawicki for helpful discussions. The referee, Daniel Stern, made a number of helpful suggestions that improved the paper. We are grateful for the

opportunity to have made these astronomical observations from the summit of Mauna Kea, a site that plays a significant cultural role within the indigenous Hawaiian community. Mark Brodwin's research has been supported by the Natural Sciences and Engineering Research Council of Canada.

REFERENCES

Barkana, R. & Loeb, A. 2000, ApJ, 539, 20
Baron, E. & White, S. D. M. 1987, ApJ, 322, 585
Becker, R. H., Fan, X., White, R. L., Strauss, M. A., Narayanan, V. K., Lupton, R. H., Gunn, J. E., Annis, J., Bahcall, N. A., Brinkmann, J., Connolly, A. J., Csabai, I., Czarapata, P. C., Doi, M., Heckman, T. M., Hennessy, G. S., Ivezic, Z., Knapp, G. R., Lamb, D. Q., McKay, T. A., Munn, J. A., Nash, T., Nichol, R., Pier, J. R., Richards, G. T., Schneider, D. P., Stoughton, C., Szalay, A. S., Thakar, A. R., & York, D. G. 2001, AJ, 122, 2850
Brodwin, M. 2003, in preparation
Bunker, A. J., Stanway, E. R., Ellis, R. S., McMahon, R. G., & McCarthy, P. J. 2003, astro-ph/0302401
Carollo, C. M. & Lilly, S. J. 2001, ApJL, 548, L153
Cen, R. 2002, ApJ, submitted, astro-ph/0210473.
Crampton, D. & Lilly, S. 1999, in ASP Conf. Ser. 191: Photometric Redshifts and the Detection of High Redshift Galaxies, 229.
Cuby, J.-G., Le Fevre, O., McCracken, H., Cuillandre, J.-C., Magnier, E., & Meneux, B. 2003, astro-ph/0303646
Dey, A., Spinrad, H., Stern, D., Graham, J., Chafee, F., 1998, ApJ, 498, L93.
Ellis, R., Santos, M. R., Kneib, J., & Kuijken, K. 2001, ApJL, 560, L119
Fan, X., and 33 co-authors, 2001, AJ, 122, 2833.
Frenk, C. S., White, S. D. M., Davis, M., & Efstathiou, G. 1988, ApJ, 327, 507
Hu, E. M., Cowie, L. L., & McMahon, R. G. 1998, ApJL, 502, L99+
Hu, E. M., Cowie, L. L., McMahon, R. G., Capak, P., Iwamuro, F., Kneib, J.-P., Maihara, T., & Motohara, K. 2002, ApJL, 568, L75
Hu, E. M., McMahon, R. G., & Cowie, L. L. 1999, ApJL, 522, L9
Kennicutt, R., 1983, ApJ, 272, 54.
Kodaira, Y., Ouchi, M., Okamura, S., & et al. 2003, PASJ, submitted
Kogut, A., Spergel, D.N., Barnes, C., Bennet C.L., Halpern, M., Hinshaw, G., Jarosik, N., Limon, M., Meyer, S.S., Page, L., Tucker, G., Wollack, E., Wright, E.L., 2003, submitted to ApJ, astro-ph/0302213
Lehnert, M.D., & Bremer, M., submitted to ApJL, astro-ph/0112431
McCarthy, P.J., ARA&A, 31, 639.
McCracken, H.J., Le Fevre, O., Brodwin, M., Foucaud, S., Lilly, S.J., Crampton, D., & Mellier, Y., 2001, ApJ, 376, 756.
Lilly, S. J., Carollo, C.M., Stockton, A.N., 2003, submitted to ApJ.
Pettini, M., Shapley, A. E., Steidel, C. C., Cuby, J., Dickinson, M., Moorwood, A. F. M., Adelberger, K. L., & Giavalisco, M. 2001, ApJ, 554, 981
Pickles, A.J., 1985, ApJS, 59, 33.
Rhoads, J. E. & Malhotra, S. 2001, ApJL, 563, L5
Rhoads, J. E., Malhotra, S., Dey, A., Stern, D., Spinrad, H., & Jannuzi, B. T. 2000, ApJL, 545, L85
Shapley, A. E., Steidel, C. C., Adelberger, K. L., Dickinson, M., Giavalisco, M., & Pettini, M. 2001, ApJ, 562, 95
Stanway, E., Bunker, A., & McMahon, R. 2003, MNRAS, in press
Steidel, C. C., Giavalisco, M., Pettini, M., Dickinson, M., & Adelberger, K. L. 1996, ApJL, 462, L17
Steidel, C.C., Hunt, M.P., Shapley, A., Adelberger, K.L., Pettini, M., Dickinson, M., Giavalisco, M., 2002, ApJ, 576, 653.
Stern, D., Dey, A., Spinrad, H., Maxfield, L., Dickinson, M., Schlegel, D., Gonz· lez, R.A., 1999, AJ, 117, 1122.
Stern, D., Bunker, A., Spinrad, H., Dey, A., 2000, ApJ, 537, 73.
Stockton, A. 1999, Ap&SS, 269, 209
Weinberg, D. H., Hernquist, L., & Katz, N. 2002, ApJ, 571, 15
Yan, H., Windhorst, R. A., & Cohen, H. 2003, ApJL, in press